THE JOURNAL OF PHYSICAL CHEMISTRY B

ARTICLE

pubs.acs.org/JPCB

Optical Heterodyne-Detected Raman-Induced Kerr Effect (OHD-RIKE) Microscopy

Christian W. Freudiger,[†,‡,∥] Maarten B. J. Roeffaers,[†,∥,⊥] Xu Zhang,[†,§] Brian G. Saar,[†,¶] Wei Min,[†,√] and X. Sunney Xie*[,†]

[†]Department of Chemistry and Chemical Biology, Harvard University, Cambridge, Massachusetts 02138, United States

[‡]Department of Physics, Harvard University, Cambridge, Massachusetts 02138, United States

[§]Department of Applied Physics, Harvard University, Cambridge, Massachusetts 02138, United States

ABSTRACT: Label-free microscopy based on Raman scattering has been increasingly used in biomedical research to image samples that cannot be labeled or stained. Stimulated Raman scattering (SRS) microscopy allows signal amplification of the weak Raman signal for fast imaging speeds without introducing the nonresonant background and coherent image artifacts that are present in coherent anti-Stokes Raman scattering (CARS) microscopy. Here we present the Raman-induced Kerr effect (RIKE) as a contrast for label-free microscopy. RIKE allows us to measure different elements of the nonlinear susceptibility tensor, both the real and imaginary parts, by optical heterodyne detection (OHD-RIKE). OHD-RIKE microscopy provides information similar to polarization CARS (P-CARS) and interferometric CARS (I-CARS) microscopy, with a simple modification of the two-beam SRS microscopy setup. We show that, while OHD-RIKE microspectroscopy can be in principle more sensitive than SRS, it does not supersede SRS microscopy of heterogeneous biological samples, such as mouse skin tissue, because it is complicated by variations of linear birefringence across the sample.

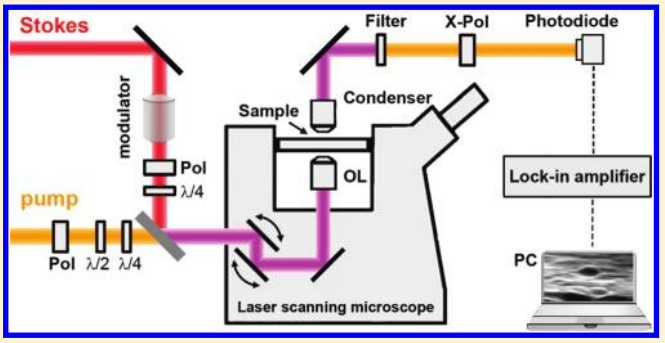

I. INTRODUCTION

Recently, a variety of label-free microscopy techniques have been developed for imaging of samples which cannot be labeled or stained with fluorophores or dyes. Vibrational spectroscopy is especially useful for chemical imaging, as every molecule has a specific vibrational fingerprint.[1,2] However, infrared absorption (IR) is hindered by low spatial resolution and spontaneous Raman by weak signal levels, limiting imaging speed and sensitivity in microscopy.

In coherent anti-Stokes Raman scattering (CARS) microscopy,[3,4] the sample is excited with two laser beams at the pump frequency, ω_p, and the Stokes frequency, ω_S. If the difference frequency $\Delta\omega = \omega_p - \omega_S$ is tuned into a vibrational frequency Ω of the sample, a strong signal is generated at the new anti-Stokes frequency, $\omega_{aS} = 2\omega_p - \omega_S$, which is enhanced by orders of magnitude compared to spontaneous Raman scattering[5,6] and allows for fast imaging at speeds up to video-rate.[7]

CARS microscopy has however been limited by the presence of a nonresonant background, which is generated even without resonant molecules in the focus. It causes spectral distortion of the Raman spectrum,[8] image artifacts, and limited sensitivity.[9] Quantification of CARS images further suffers from a nonlinear dependence on the concentration of the target molecule[10] and coherent image artifacts.[11]

Stimulated Raman scattering (SRS)[6,12,13] overcomes all of these problems.[14−17] It is present simultaneously with CARS and manifests as intensity gain (stimulated Raman gain, SRG) and loss (stimulated Raman loss, SRL) of the transmitted excitation beams. To extract the signal with high sensitivity, we have implemented a high-frequency phase-sensitive detection scheme by modulating the Stokes beam intensity at 10−20 MHz and detecting the modulation transfer to the pump beam with a lock-in amplifier. Because laser noise and fluctuations due to varying sample transmission during beam-scanning primarily occur at low frequencies, close to shot-noise limited sensitivity can be readily achieved.[15] Recently, video-rate *in vivo* SRS imaging in the epi-direction[18] and the combination of the high-frequency detection scheme with multiplex excitation[19] has been demonstrated, making SRS microscopy a more valuable contrast for microscopy.

The original implementations of SRS microscopy[15,18] have been focused on mapping the distribution of the spontaneous Raman cross section, σ, and polarization sensitive measurements, such as the Raman depolarization ratio, ρ, are not made. This has previously been possible with polarization-sensitive CARS (P-CARS) microscopy[20,21] and can provide additional information

Special Issue: Shaul Mukamel Festschrift

Received: November 30, 2010
Revised: March 18, 2011
Published: April 19, 2011

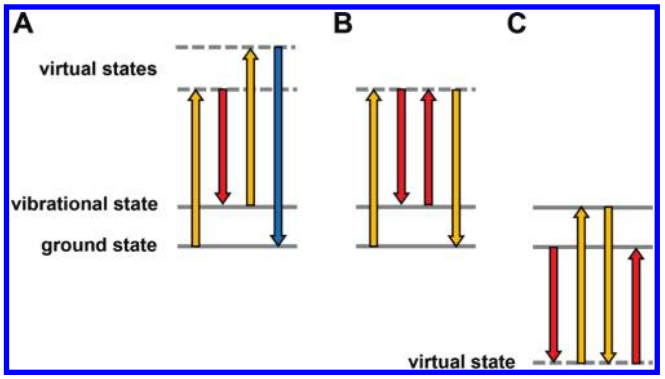

Figure 1. Coherent Raman scattering techniques. Energy diagrams of (A) CARS, (B) SRL and RIKE of the pump beam, and (C) SRG and RIKE of the Stokes beam. All processes probe the vibrational excited state of the molecules in focus. Virtual states originate from the electronic response, are instantaneous, and thus can have an undefined energy different from the eigenstates of the system (even negative as in part C). Different directions of the emission light indicate different phase relationships with the excitation beams.

about the local molecular orientation and symmetries in the sample, e.g., in myelinated axons[22] and cellulose fibers.[23]

SRS also intrinsically probes the imaginary part of the nonlinear susceptibility tensor $\chi^{(3)}$ and does not allow accessing its real part as interferometic CARS (I-CARS) techniques.[24−27] While Raman-based chemical imaging techniques generally aim to extract the imaginary part,[24,25] which carries the specific vibrational information only, imaging the real part of the nonlinear response of the sample might have important applications, such as the label-free detection of neuronal activity.[28]

Here we present the Raman-induced Kerr effect (RIKE),[5,6,29] which has been widely used in spectroscopy,[30−33] as a contrast mechanism for microscopy.[34] Similar to P-CARS, RIKE allows mapping of different elements of $\chi^{(3)}$, however without the disadvantages of CARS. Similar to I-CARS, both the real and imaginary part of $\chi^{(3)}$ can be probed by optical heterodyne detection (OHD-RIKE), however in a more straightforward two-beam geometry. OHD-RIKE has also been found to be more sensitive than SRS in spectroscopy,[6] because the strength of the local oscillator can be adjusted to reduce laser noise.

II. THEORETICAL BACKGROUND

RIKE as a Coherent Raman Scattering (CRS) Technique. All CRS techniques, including CARS, SRS, and RIKE, can be understood as four-wave mixing processes, in which emission is generated from a third order polarization due to the nonlinear interaction of the excitation fields with the sample (Figure 1).[6,35] CARS generates an electric field at the anti-Stokes frequency, ω_{aS}, SRS induces an intensity gain (stimulated Raman gain, SRG) and loss (stimulated Raman gain, SRL) of the excitation beams, and the RIKE changes the polarization of one of the excitation beams due to the Raman-induced birefringence in the sample. In both SRS and RIKE, the generated emission is thus at the excitation frequencies. In SRS, this radiation is emitted parallel to the excitation field, and in RIKE, the emission is polarized perpendicular to the excitation fields. In this aspect, RIKE is similar to CARS, as the emitted radiation does not interfere with the excitation light, while in SRS interference of the new emission results in intensity gain or loss of the excitation fields.

Generally, the polarization of the sample can be written as a power series of the excitation fields. The general expression for the third order contribution at the frequency ω_4 is

$$P^{(3)}(\omega_4) = \chi^{(3)}(\omega_4;\omega_1,\omega_2,\omega_3)\cdot E(\omega_1)\cdot E(\omega_2)\cdot E(\omega_3) \quad (1)$$

where $\chi^{(3)}(\omega_4;\omega_1,\omega_2,\omega_3)$ is the nonlinear optical susceptibility and $E(\omega_1)$, $E(\omega_2)$, and $E(\omega_3)$ are the electric fields of the excitation beams at ω_1, ω_2, and ω_3.[6] In this notation, CARS excitation is at $\omega_1 = \omega_3 = \omega_p$ and $\omega_2 = -\omega_S$ and emission is at $\omega_4 = -\omega_{aS}$. In SRL and its analogue in RIKE, excitation is at $\omega_1 = \omega_p$ and $\omega_2 = -\omega_3 = -\omega_S$ and emission is at $\omega_4 = -\omega_p$. In SRG and its analogue in RIKE, excitation is at $\omega_1 = -\omega_S$ and $\omega_2 = -\omega_3 = \omega_p$ and emission is at $\omega_4 = \omega_S$. We note that in the notation ω_S, ω_p and ω_{aS} are positive numbers and the negative signs account for opposite phase as indicated by the direction of the arrows in the energy diagrams in Figure 1.

All CRS techniques share the common feature that $\Delta\omega = \omega_1 + \omega_2 = \omega_p - \omega_S$ can be tuned to match a vibrational resonance of the sample with center frequency Ω. All spectroscopic information is contained in $\chi^{(3)}$, which, far from electronic resonance, has a nuclear contribution $\chi_r^{(3)}$ and electronic contribution $\chi_{nr}^{(3)}$:

$$\chi^{(3)} = \mp(\chi_r^{(3)} + \chi_{nr}^{(3)}) = \mp\left(\frac{A}{\Omega - \Delta\omega - i\cdot\Gamma} + \chi_{nr}^{(3)}\right) \quad (2)$$

where A is proportional to the particular spontaneous Raman cross section and Γ is the half-width at half-maximum.[35,36] Because the electronic response does not probe the vibrational resonance and is instantaneous, $\chi_{nr}^{(3)}$ is independent of $\Delta\omega$ and purely real. The resonant contribution $\chi_r^{(3)}$ has real and imaginary components, which results in a phase shift of the nonlinear polarization with respect to the excitation fields. In particular, as indicated by the positive and negative signs in eq 2, on resonance, the nonlinear polarization has a relative phase of −90° with respect to the excitation fields for CARS and SRL and 90° for SRG. The imaginary part has a typical Lorentzian line shape of spontaneous Raman spectra, and the real part has a dispersive character.[35,36]

This nonlinear polarization further has to be treated as a tensor $\chi^{(3)}_{\alpha\beta\gamma\delta}$, in which α, β, γ, and δ are the indices of the polarization components of the electrical fields $E_\alpha(\omega_1)$, $E_\beta(\omega_2)$, $E_\gamma(\omega_3)$, and $E_\delta(\omega_4)$ in the x-, y-, and z-direction. Depending on the symmetry of the system, only certain combinations are allowed. Specifically, in isotropic samples $\chi^{(3)}_{1111}$, $\chi^{(3)}_{1122}$, $\chi^{(3)}_{1212}$, and $\chi^{(3)}_{1221}$ and their permutations are the only nonvanishing elements and their resonant contributions can be related to σ and ρ.[6]

In the original implantation of SRS microscopy, parallel and linearly polarized excitation fields were used; i.e., features of $\chi^{(3)}_{1111}$ were measured (see Figure 2). It is straightforward to also measure features of $\chi^{(3)}_{1221}$ by using linearly polarized pump and Stokes beams with perpendicular polarization. In the SRL analogue of RIKE, the emission is perpendicular to the original polarization of the pump beam, which we detect by blocking the transmitted pump beam with a cross-polarizer and measuring the polarization rotation due to the nonlinear interaction with the sample (see experimental section). Traditionally, two different beam geometries have been routinely used: one employs a linearly polarized Stokes beam at a 45° angle with respect to pump beam (known as linear RIKE), the other uses a circularly

dx.doi.org/10.1021/jp1113834 |J. Phys. Chem. B 2011, 115, 5574–5581

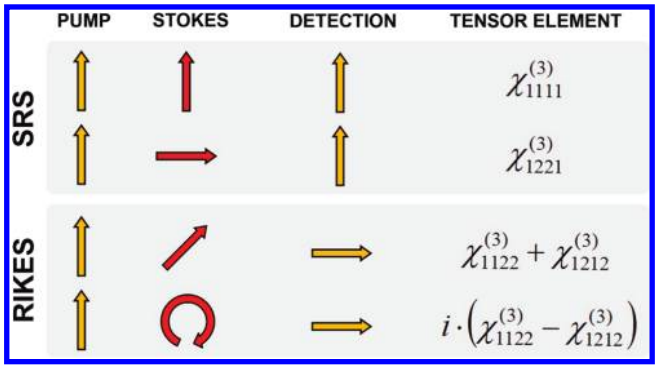

Figure 2. Polarization configurations for SRS and RIKE of the pump beam. The first two columns show the polarization of the excitation fields (pump and Stokes) and the third column the orientation of a polarizer in front of the detector, which is sensitive for the pump beam only. Configurations in which detection is along the polarization of the pump beam are referred to as SRS, and configurations in which detection is perpendicular to the polarization of the pump beam as RIKE. In isotropic samples, $\chi^{(3)}_{1111}$, $\chi^{(3)}_{1122}$, $\chi^{(3)}_{1212}$, and $\chi^{(3)}_{1221}$ are the nonvanishing elements of the third order susceptibility tensors, so only the four configurations shown here generate a signal. RIKE requires the Stokes beam to have polarizations along both polarization axes. One can distinguish between linear RIKE, in which both polarizations have the same phase, and circular RIKE, in which one of the polarizations is shifted by 90°. The fourth column indicates the specific tensor elements that are probed.

polarized Stokes beam (known as circular RIKE) (see Figure 2). The RIKE nonlinear polarization at the pump frequency is proportional to $\chi^{(3)}_{1122}+\chi^{(3)}_{1212}$ for the linear RIKE and $i\cdot(\chi^{(3)}_{1122}-\chi^{(3)}_{1212})$ in case of the circularly RIKE, where i indicates that the polarization is phase-shifted by 90° with respect to the phase of the pump beam.[6] Thus, the combination of SRS and RIKE microscopy can probe the distribution of all important tensor elements of the nonlinear susceptibility in the sample.[6]

Optical Heterodyne Detection in CRS. Theoretically RIKE, in contrast to SRS, is a background-free technique as the emission is polarized perpendicular to the excitation light, which is blocked with a cross-polarizer. In practice, however, and especially in a microscopy configuration with a high numerical aperture (NA) objectives,[20] it is hard to suppress the excitation light sufficiently. It is thus useful to introduce a carefully controlled portion of the excitation light, e.g. by detuning either the cross-polarizer with respect to the excitation beams or the excitation beams with respect to the cross-polarizer. Due to the coherent nature of RIKE, this portion of the transmitted excitation light interferes with the RIKE emission. Such approach is known as optical heterodyne detected RIKE (OHD-RIKE).[6,29]

Optical heterodyne detection is a standard technique in spectroscopy.[6,37] The general idea is that the small homodyne signal $E^{(3)}$ is amplified with a second, coherent electrical field at the same frequency E_{LO}, known as the local oscillator. Because of the coherent addition of the two fields, the overall detected intensity is proportional to

$$|E_{\mathrm{LO}}+E^{(3)}|^2 = |E_{\mathrm{LO}}|^2 + 2\cdot\mathrm{Re}[E_{\mathrm{LO}}]\cdot\mathrm{Re}[E^{(3)}] + 2\cdot\mathrm{Im}[E_{\mathrm{LO}}]\cdot\mathrm{Im}[E^{(3)}] + |E^{(3)}|^2 \quad (3)$$

If $|E_{LO}|\gg|E^{(3)}|$, the contribution due to the homodyne signal $|E^{(3)}|^2$ is negligible compared to the mixing term $\mathrm{Re}[E_{LO}]\cdot\mathrm{Re}[E^{(3)}]+\mathrm{Im}[E_{LO}]\cdot\mathrm{Im}[E^{(3)}]$. If heterodyne detection is further combined with a modulation transfer scheme as used in SRS microscopy (see experimental section), the contribution of the local oscillator $|E_{LO}|^2$ is suppressed and only the mixing terms are detected. Depending on the phase of E_{LO}, the real and imaginary part of $E^{(3)}$ can be probed specifically by seting either $\mathrm{Re}[E_{LO}]$or $\mathrm{Im}[E_{LO}]$ to zero.

In CRS, the small homodyne signal $E^{(3)}$ is the radiation generated from the nonlinear polarization $P^{(3)}(\omega_4)$. It turns out that $E^{(3)}$ is 90° phase-shifted with respect to $P^{(3)}(\omega_4)$ (see eq 4.75 in reference[37]) and thus

$$\mathrm{Re}[E^{(3)}] \propto \mathrm{Im}[\chi^{(3)}]\cdot E(\omega_1)\cdot E(\omega_2)\cdot E(\omega_3) \quad (4a)$$

$$\mathrm{Im}[E^{(3)}] \propto -\mathrm{Re}[\chi^{(3)}]\cdot E(\omega_1)\cdot E(\omega_2)\cdot E(\omega_3) \quad (4b)$$

with $E(\omega_1)$, $E(\omega_2)$, and $E(\omega_3)$ being real by definition. As such the signal in optically heterodyne detected CRS is proportional to

$$(\mathrm{Re}[E_{\mathrm{LO}}]\cdot\mathrm{Im}[\chi^{(3)}] - \mathrm{Im}[E_{\mathrm{LO}}]\cdot\mathrm{Re}[\chi^{(3)}])\cdot E(\omega_1)\cdot E(\omega_2)\cdot E(\omega_3) \quad (5)$$

In CARS microscopy, optical heterodyne detection has been performed previously by providing the local oscillator in the form of a third beam at ω_{aS} in the excitation light to measure real and imaginary part of the nonlinear susceptibility and suppress the nonresonant background.[21,24−26] This is challenging experimentally because it requires generation of a third wavelength and precise phase control of three laser beams in a beam-scanning microscope. In SRS and OHD-RIKE, optical heterodyne detection can be performed without the need for a third beam, as the coherent emission from the sample occurs at the excitation frequencies.

SRS is actually a very special case of intrinsic optical heterodyne detection as both frequency and polarization of the new emission generated from the nonlinear polarization are identical to that of the transmitted excitation beam. For this reason, the local oscillator is strong and $\mathrm{Im}[E_{LO}] = 0$ by definition. Thus SRS intrinsically probes $\mathrm{Im}[\chi^{(3)}]$. This explains why SRS microscopy does not suffer from a nonresonant background as $\mathrm{Im}[\chi^{(3)}_{nr}] = 0$ due to the instantaneous electronic response. Thus even though $\chi^{(3)}_{nr}\neq 0$, it is not detected in SRS microscopy, since the nonresonant background does not interfere with the excitation fields and thus is not amplified by optical heterodyne detection. It further explains why SRS spectra are identical to those of spontaneous Raman scattering, which also probes $\mathrm{Im}[\chi^{(3)}]$.[6,14,15]

In RIKE the emitted homodyne field from the sample has the same frequency as the excitation fields but occurs at the perpendicular polarization and could thus be detected in a background-free manner. In OHD-RIKE some of the excitation beam is rotated to match the emission polarization, allowing us to provide a local oscillator with adjustable strength and phase. In contrast to SRS, in OHD-RIKE the local oscillator strength can thus be optimized and both the real and imaginary parts of the nonlinear susceptibility tensor can be probed selectively

III. EXPERIMENTAL SETUP

The instrumentation required for OHD-RIKE microscopy is based on a typical SRS microscope with high-frequency

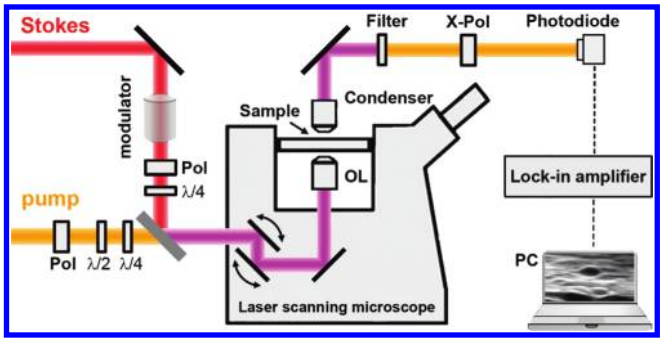

Figure 3. Experimental setup for circular OHD-RIKE microscopy. The pump and Stokes beam are provided by a mode-locked Nd:YVO_4 laser at 1064 nm (Stokes beam), which synchronously pumps an optical parametric oscillator with tunable output from 650 to 1020 nm (pump beam). The amplitude of the Stokes beam is modulated with a resonant Pockels cell, spatially overlapped with the pump beam with a dichroic mirror (DM) and aligned into a laser scanning microscope. Collinear beams are focused by the objective lens (OL) into the sample. Transmitted beams are collected with a condenser. After blocking the Stokes beam with a filter, the intensity of the pump beam is detected with a photodiode. A lock-in amplifier measures the amplitude of the modulation transfer to the pump beam due to the nonlinear interaction with the sample to provide the intensity of a pixel. For OHD-RIKE, the pump and Stokes beams are first linearly polarized with polarizers (Pol) and a cross-polarizer (X-Pol) is inserted in front of the photodiode to block the transmitted pump beam. The exact position is set by the intensity dependence after a polarizer. For circular RIKE, the Stokes beam is circular polarized with a quarter-wave plate ($\lambda/4$), which would be replaced by a half-wave plate for linear RIKE. For OHD-RIKE, we install a half-wave plate ($\lambda/2$) in the pump beam path to adjust the amount of transmitted light through the cross-polarizer in order to control the strength of the local oscillator. The phase of the local oscillator can be shifted by 90° to selectively probe the imaginary part of the nonlinear response by a quarter-wave plate ($\lambda/4$) in the pump path along the axis of the local oscillator.

phase-sensitive detection.[15] Here we describe how such SRS microscope can be modified to perform OHD-RIKE.

Experimental Setup for SRL Microspectroscopy and Microscopy. The experimental apparatus is shown in Figure 3. Synchronized, mode-locked laser pulse-trains are provided by an optical parametric oscillator (OPO) (Levante Emerald, APE-Berlin) synchronously pumped by a frequency doubled Nd:YVO_4 laser (High-Q, picoTRAIN). Additionally, this laser provides a separate output of the fundamental beam at 1064 nm. The 1064 nm beam is used as the Stokes beam in combination with the signal beam from the OPO as the pump beam for CRS. The beams are spatially overlapped with a dichroic beam-combiner (Chroma Technology, 1064 DCRB). The Stokes beam is modulated with a home-built Pockel Cell (crystal from Raicol) and resonantly driven at 10 MHz by the internal clock of a lock-in amplifier (Stanford Research Systems, SR844RF). This home-built Pockel cell has the advantage that the RF drive signal is amplified within the same electrically shielded box that contains the modulator crystal to minimize radio frequency emission that can be detected by the lock-in amplifier. A polarization-analyzer is used to transform the polarization modulation of the Pockel cell into amplitude-modulation.

Pump and Stokes beams are coupled into a modified upright laser scanning microscope (Olympus, BX61WI/FV300) optimized for IR transmission. A 60x 1.2 NA water objective (Olympus, UPlanApo/IR) is used as excitation objective and light is collected in transmission with a 1.4 NA oil condenser (Nikon). After blocking the Stokes beam with a bandpass filter (Chroma, CARS 890/220) the pump beam is detected with a large-area photodiode (Thorlabs, FDS1010) which is reverse-biased to 64 V. The photodiode output is bandpass-filtered (Mini-Circuits, BBP-10.7) to suppress the strong high-frequency signal due to the laser pulsing (76 MHz) and the low-frequency signal from scanning the beams through the sample with varying transmission. The high-frequency lock-in amplifier that drives the Pockel cell is used to demodulate the pump intensity.

For imaging, the output of the lock-in amplifier is fed into the A/D-converter of the microscope to provide the pixel intensity. For the microspectroscopy, an RS232 computer-controlled interface of the OPO was developed in collaboration with APE GmbH. In brief, the OPO wavelength is tuned with the in cavity Lyot-filter within the phase-matching bandwidth of LBO crystal at a given temperature, allowing up to 200 cm^{-1} tuning range. The microscope is set to illuminate a fixed position in the sample, the OPO is tuned, and the intensity from the lock-in amplifier for each $\Delta\omega$ is recorded.

Modifying an SRS Microscope to Perform OHD-RIKE. We implement the SRL analogue of OHD-RIKE by detecting the polarization rotation of the pump beam due to the nonlinear interaction with the Stokes beam in the focus. First, two polarizers (Thorlabs, GTH5M) are used to linearly polarize the pump and Stokes beams. A crossed polarizer (Thorlabs, LPVIS100) is placed in front of the photodiode and positioned to minimize transmission. Due to the inherent loss of depolarization of tightly focused beams, the best extinction ratio that could be achieved is 1:300.

A half-waveplate (Thorlabs, WPH05M-1064) or a quarter-waveplate (Thorlabs, WPQ05M-1064) is placed in the Stokes beam to produce linearly polarized Stokes light at a polarization of 45° with respect to the pump beam or circularly polarized Stokes light for linear or circular OHD-RIKE, respectively. Special care was taken to ensure the exact positions of the waveplates. The position of the waveplate can further be optimized using the spectral property of the OHD-RIKE signal; e.g., in circular OHD-RIKE, the nonresonant signal due to cross-phase modulation was zeroed.

To control the amplitude of the local oscillator for heterodyne detection, a half-waveplate (Thorlabs, AHWP05M-980) slightly rotates the polarization of the linear pump beam such that a portion of the light passes through the polarizer in front of the detector. The strength of the local oscillator is measured by recording the DC current from the photodiode.

The phase of the local oscillator can be continuously controlled using a Babinet−Soleil compensator (OFR, SB-10) aligned along the polarization of the local oscillator. Thus, by tuning the phase delay, it is possible to specifically access the real and imaginary components of the emitted radiation. In linear OHD-RIKE, the nonlinear polarization is in phase with the excitation pump field (see Figure 2) and the imaginary part of $\chi^{(3)}_{1122} + \chi^{(3)}_{1212}$ can be probed with no phase delay in the local oscillator. In circular OHD-RIKE, the nonlinear polarization is 90° phase-shifted with respect to the excitation pump field (see Figure 2). Thus, to probe the imaginary part of $\chi^{(3)}_{1122} - \chi^{(3)}_{1212}$, the local oscillator has to also be phase-shifted by 90°, i.e., a quarter-wave. To probe the real part of $\chi^{(3)}_{1122} + \chi^{(3)}_{1212}$ and $\chi^{(3)}_{1122} - \chi^{(3)}_{1212}$, the local oscillator has to be shifted by 90 or 0° in linear and circular RIKE, respectively. Thus, in these special cases, the

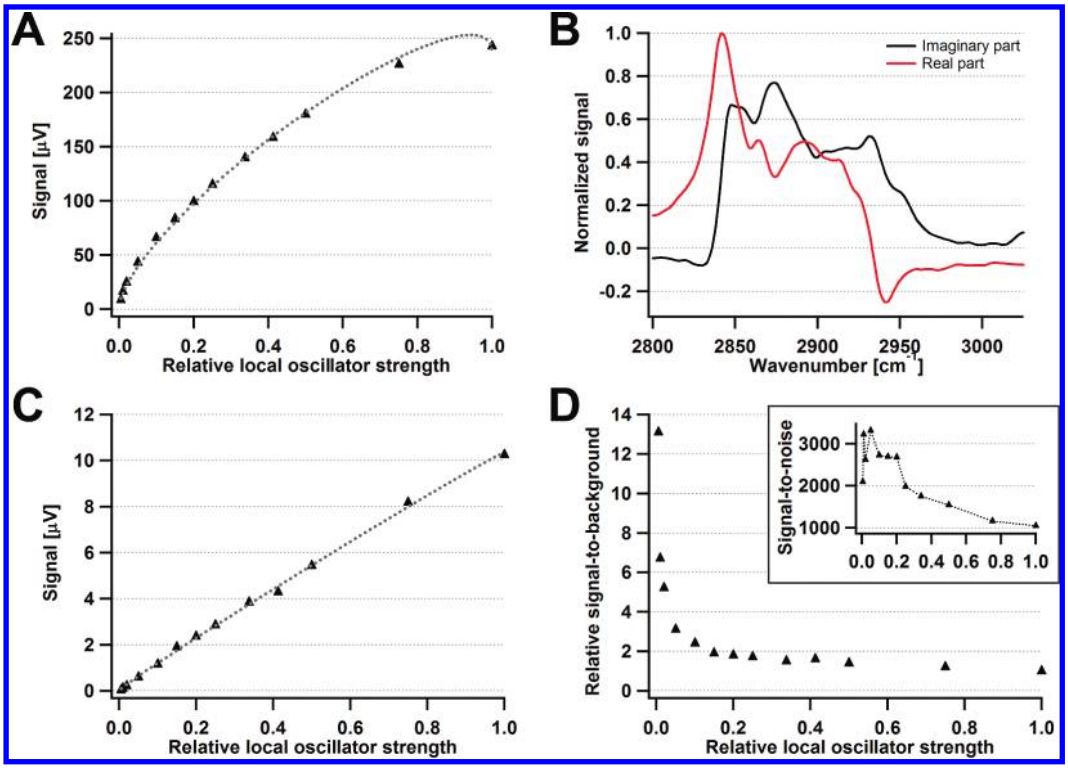

Figure 4. OHD-RIKE microspectroscopy. (A) OHD-RIKE signal of methanol at 2830 cm^{-1} as a function of the local oscillator strength relative to the total pump beam intensity. The dashed line is the fit with eq 6. (B) OHD-RIKE spectra of dodecane with the phase of the local oscillator set to probe the real (red line) and imaginary part (black line) of the nonlinear susceptibility tensor. (C) Cross-phase modulation of water at 2830 cm^{-1} as a function of the local oscillator strength. The dashed line is the fit with eq 6. (D) Ratio of methanol signal (shown in part A) to cross-phase modulation background (shown in part C) normalized to by the signal from SRS. Inset: signal-to-noise ratio of the signal of pure methanol (shown in part A) over the noise of the cross-phase modulation signal in part C.

Babinet−Soleil compensator is not necessary, as either no phase delay is needed at all (0° phase shift) or a simple achromatic quarter-wave plate (Thorlabs, AQWP05M-980) is sufficient (90° phase shift).

IV. RESULTS

Signal Dependence on Local Oscillator Strength. One of the differences of OHD-RIKE compared to SRS is that the strength of the local oscillator can be controlled. Figure 4A shows the circular OHD-RIKE signal of methanol at 2830 cm^{-1} as a function of the intensity of the local oscillator strength. The microscope was configured to probe $\mathrm{Im}[\chi^{(3)}_{1122} - \chi^{(3)}_{1212}]$; i.e., the phase of the local oscillator was set such that $\mathrm{Im}[E_{\mathrm{LO}}] = 0$.

With $\alpha = I_{\mathrm{LO}}/I_{\mathrm{pump}}$, where I_{LO} is the measured intensity of the local oscillator transmitted through the cross-polarizer and I_{pump} is the total intensity of the pump beam, $E_{\mathrm{LO}} \propto (\alpha)^{1/2}$ and $E(\omega_1) \propto (1 - \alpha)^{1/2}$, because with increasing intensity of the local oscillator the intensity of the other polarization component of the pump field is depleted by the same amount. According to eq 5, the intensity of OHD-RIKE is thus proportional to $\mathrm{Im}[\chi^{(3)}_{1122} - \chi^{(3)}_{1212}] \cdot (1 - \alpha)^{1/2} \cdot (\alpha)^{1/2}$.

With increasing local oscillator strength, the measured signal is however not only originating from the OHD-RIKE process but also from the SRS signal of the local oscillator itself, which is proportional to the intensity of the local oscillator α. Since the Stokes beam is circularly polarized, the SRS signal of the local oscillator is further proportional to $\mathrm{Im}[\chi^{(3)}_{1111} + \chi^{(3)}_{1221}]$. Thus, theoretically, the intensity dependence of the overall measured signal is

$$\alpha \cdot S_{\mathrm{SRS}} + (\sqrt{\alpha} \cdot \sqrt{1 - \alpha}) \cdot S_{\mathrm{RIKE}} \qquad (6)$$

with proportionality constants S_{SRS} and S_{RIKE}, which can be related to $Im[\chi^{(3)}_{1122} - \chi^{(3)}_{1212}]$ and $\mathrm{Im}[\chi^{(3)}_{1111} + \chi^{(3)}_{1221}]$, respectively.

The theoretical prediction describes the experimental results well, and fitting the data for the 2830 cm^{-1} vibration of methanol shows that $S_{\mathrm{SRS}}/S_{\mathrm{RIKE}} = 1.9$. If the local oscillator is 1% of the pump beam intensity, the signal contribution from RIKE is thus about 5× stronger than the signal from SRS.

OHD-RIKE Microspectroscopy. By controlling the phase of the local oscillator with the Babinet−Soleil compensator, it is possible to access both real and imaginary parts of the nonlinear susceptibility. Figure 4B shows both $\mathrm{Re}(\chi^{(3)}_{1122} - \chi^{(3)}_{1212})$ and $\mathrm{Im}(\chi^{(3)}_{1122} - \chi^{(3)}_{1212})$ of the CH-stretching vibrational spectrum for dodecane measured with circular RIKE with the phase set to 0 and 90°, respectively, and 1% of the pump intensity in the local oscillator. The lock-in amplifier was set such that a loss of the pump intensity appears as a positive signal (i.e., SRL causes a positive signal). As such, the positive and negative signals in $\mathrm{Re}(\chi^{(3)}_{1122} - \chi^{(3)}_{1212})$ correspond to loss or gain of the local oscillator intensity.

Overcoming Cross-Phase Modulation. In general, chemical imaging aims to detect the resonant response of the sample, i.e., the imaginary part of the nonlinear response, which carries the chemically specific information. Whereas in CARS microscopy this weak resonant response can be overwhelmed by the

dx.doi.org/10.1021/jp1113834 |J. Phys. Chem. B 2011, 115, 5574–5581

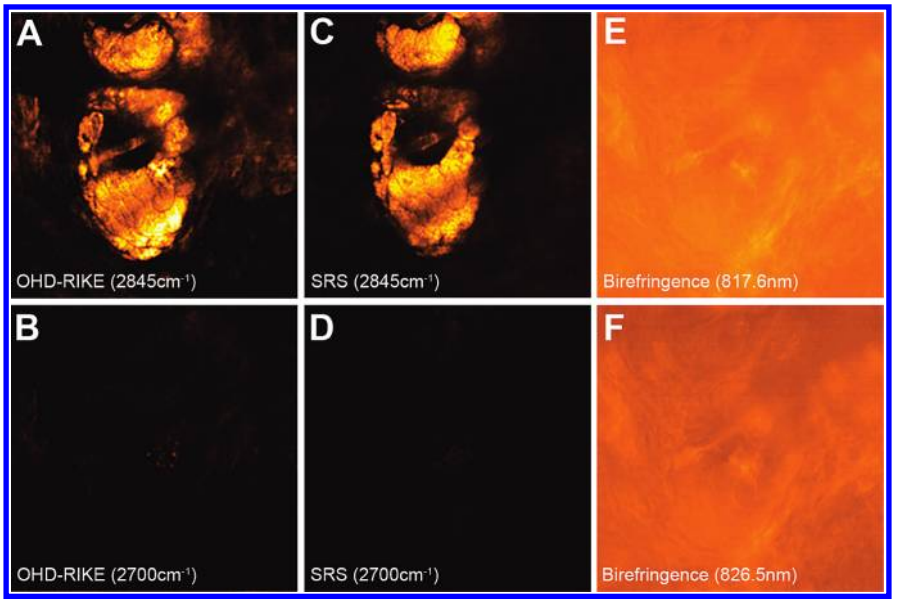

Figure 5. OHD-RIKE microscopy. (A) OHD-RIKE image of a sebaceous gland in the viable epidermis of mouse skin tuned into the CH_2-streching vibration of lipids (2845 cm^{-1}) and (B) tuned off vibrational resonance (2700 cm^{-1}). (C and D) SRS images of the same region both on and off resonance, respectively. (E and F) Linear birefringence image of the same region at 817.6 and 826.5 nm, respectively. In the OHD-RIKE images, image contrast tuned off vibrational resonance mainly vanishes except in areas of increased local oscillator due to the linear birefringence of the sample.

nonresonant background, SRS has improved the detection sensitivity of label-free microscopy by overcoming this notorious background signal. However, another, much weaker, spurious background signal from cross-phase modulation (XPM) can be the limiting factor when pushing the sensitivity limit to low chemical concentrations.[15,38]

XPM is detected in SRS microscopy because the modulated Stokes beam intensity causes a modulation of the refractive index in focus due to the Kerr effect. This results in a modulation of the divergence of the transmitted pump beam. If the pump beam, after passing through the focus, strikes any type of aperture (e.g., the edges of the collection optics), this divergence modulation is transformed into an amplitude modulation which is detected by the lock-in amplifier. As such, the modulated change of focusing properties can cause a spurious background signal in SRS microscopy. Using a condenser with numerical aperture (NA = 1.4) higher than that of the excitation objective (NA = 1.2) and a large area photodiode in order to collect all the light from the sample minimizes this effect.[15] However, in strongly scattering samples, this is not always possible and XPM cannot always be fully suppressed.

In OHD-RIKE microscopy set to probe the imaginary part of $\chi^{(3)}$, the same process can also cause spurious background signal proportional to $\mathrm{Re}(\chi^{(3)}_{1122} \pm \chi^{(3)}_{1212})$. However, the off vibrational resonance is $\chi^{(3)}_{1122} = \chi^{(3)}_{1212} = \chi^{(3)}_{1221} = (1/3)\chi^{(3)}_{1111}$ according to Kleinmann symmetry.[6] Thus, circular OHD-RIKE should be free of spurious background signal from XPM as $\mathrm{Re}(\chi^{(3)}_{1122} - \chi^{(3)}_{1212}) = 0$.

In order to check this hypothesis, we measure the XPM signal from water (off resonance of the OH-stretching vibration at 2830 cm^{-1}) as a function of the local oscillator strength (Figure 4C). We measure XPM by placing a pinhole in front of the detector to effectively reduce the collection NA. Fitting eq 6 to this data confirms that $S^{\mathrm{XPM}}_{\mathrm{RIKE}} \ll S^{\mathrm{XPM}}_{\mathrm{SRS}}$ and all the detected signal originates from the XPM of the local oscillator which probes $\mathrm{Re}(\chi^{(3)}_{1111} + \chi^{(3)}_{1221}) \neq 0$. Thus, it is shown here that the off vibrational resonance Kleinmann symmetry is obeyed for the used mid-IR lasers and that circular OHD-RIKE can indeed overcome XPM.

Figure 4D shows the ratio of the detected OHD-RIKE signal of methanol over the XPM background signal of water with a closed pinhole in front of the detector as a function of local field strength. At small local fields, the majority of the detected signal originates from RIKE and hence the signal-to-background is much better than that for SRS.

The inset shows the resulting signal-to-noise ratio of the resonant methanol signal over the noise of the XPM background signal from water with closed pinhole as a function of local field strength. The signal-to-noise at maximal local field corresponds to the one of SRS with a circular Stokes beam, which is less than that for SRS with minimal XPM with a high-NA objective.[15] In the regime of large local fields, the noise is mainly determined by the intensity fluctuations of the nonresonant XPM signal due to laser intensity fluctuations. Therefore, it follows the trend of the signal-to-background ratio. In the regime of small local fields, it is determined by electrical noise which is independent of signal and the signal-to-noise ratio decreases with decreasing signal. At the maximum, the signal-to-noise is improved by about 3× compared to circular SRS. The sensitivity at low local fields could be further improved by using more advanced detection electronics (e.g., resonant tank circuit) or by using an avalanche photodiode; however, as discussed in the following section, this regime is typically not reached in microscopy.

OHD-RIKE Microscopy. Figure 5A shows a circular OHD-RIKE image of a sebaceous gland surrounding a hair follicle in mouse skin at the CH_2-stretching vibration of the lipids at 2845 cm^{-1}. By tuning off resonance (Figure 5B), the image contrast vanishes; however, a few features do not disappear. They can be explained because of the linear birefringence of the sample which creates a local oscillator of uncontrolled phase. The images of the intensity of the local oscillator (Figure 5E and F) show that even though the local oscillator was set to 1% of the pump

dx.doi.org/10.1021/jp1113834 |J. Phys. Chem. B 2011, 115, 5574–5581

intensity in the local oscillator prior to the imaging, locally up to 5% of the pump beam can be transmitted through the cross-polarizer due to the spatially varying birefringence of the sample.

Figures 5C and D show the comparison with SRS imaging of the same region of tissue. While XPM introduces a spurious background signal, these effects are weaker than the background effects due to linear birefringence in RIKE and much weaker than the nonresonant background in CARS.[15]

V. DISCUSSION

In this work, we have demonstrated the Raman-induced Kerr effect (RIKE) as a contrast mechanism for label-free microscopy and shown how an existing SRS microscope can be readily modified to perform RIKE using only a few polarization optics. In this implementation, we measure the polarization rotation of the pump beam as a result of the nonlinear interaction with the Stokes beam, which can be either circularly or linearly at 45° polarized. Optical heterodyne detection is required in the microscopy implementation of RIKE to compensate for the inherent polarization loss in a tightly focused beam. In optimizing the strength of the local oscillator, we find that it has to be <1% of the intensity of the pump beam in order to detect an OHD-RIKE signal that is not overwhelmed by the SRS of the local oscillator.

Under these conditions, we find that OHD-RIKE can successfully measure different tensor elements of the nonlinear susceptibility than SRS and can determine resonant (imaginary part) and dispersive (real part) components. As such, OHD-RIKE combines the advantages of P-CARS and I-CARS microscopy; however, it utilizes a more straightforward geometry that does not require a third color beam as a local oscillator.

The motivation for us to explore OHD-RIKE was the goal to improve sensitivity compared to SRS, which was suggested by previous spectroscopy studies.[6] We show that circular RIKE is indeed free from spurious background signal due to XPM and, in principle, offers higher sensitivity than SRS, as the measurement noise scales with the spurious background signal introduced by XPM. However, OHD-RIKE microscopy suffers from similar limitations as P-CARS and I-CARS microscopy for the imaging of complex biological samples, i.e., the inherent depolarization and phase error associated in heterogeneous and birefringent samples. As such, the potential sensitivity advantages of RIKE compared to SRS are difficult to realize in practice in microscopy.

These findings further highlight why SRS[15] is a unique contrast for microscopy of biological samples. This is because SRS is a heterodyne detection scheme with a local oscillator that has the same optical frequency and polarization of the induced polarization, which avoids the complications.

AUTHOR INFORMATION

Corresponding Author

*E-mail: xie@chemistry.harvard.edu.

Present Addresses

⊥Department of Chemistry, Katholieke Universiteit Leuven, Belgium.

¶MIT Lincoln Laboratory, 244 Wood Street, Lexington, MA 02420, USA.

√Department of Chemistry, Columbia University, New York, New York, USA.

Author Contributions

‖These authors contributed equally.

ACKNOWLEDGMENT

C.W.F. acknowledges a Ph.D. fellowship from Boehringer Ingelheim Funds. M.B.J.R. acknowledges the FWO (Fondsvoor Wetenschappelijk Onderzoek) for a postdoctoral fellowship and the support from the Belgian American Educational Foundation and the Fulbright Commission - Belgium. This work was supported by the Gates Foundation and the NIH T-R01 award to X.S.X. We thank Shaul Mukamel for his many important contributions to the understanding of nonlinear optical spectroscopy.

REFERENCES

(1) Raman, C. V.; Krishnan, K. S. *Nature* **1928**, *121*, 711.
(2) Turrell, G.; Corset, J. *Raman Microscopy: Developments and Applications*; Academic Press: San Diego, CA, 1996.
(3) Zumbusch, A.; Holtom, G. R.; Xie, X. S. *Phys. Rev. Lett.* **1999**, *82*, 20.
(4) Evans, C. L.; Xie, X. S. *Annu. Rev. Anal. Chem.* **2008**, *1*, 883−909.
(5) Maker, P. D.; Terhune, R. W. *Phys. Rev.* **1965**, *137*, 3A.
(6) Levenvon, M. D.; Kano, S. S. *Introduction to Nonlinear Laser Spectroscopy*; Academic Press: San Diego, CA, 1988.
(7) Evans, C. L.; Potma, E. O.; Puoris'haag, M.; Cote, D.; Lin, C. P.; Xie, X. S. *Proc. Natl. Acad. Sci. U.S.A.* **2005**, *102*, 46.
(8) Rinia, H. A.; Bonn, M.; Muller, M. *J. Phys. Chem. B* **2006**, *110*, 9.
(9) Ganikhanov, F.; Evans, C. L.; Saar, B. G.; Xie, X. S. *Opt. Lett.* **2006**, *31*, 12.
(10) Li, L.; Wang, H. F.; Cheng, J. X. *Biophys. J.* **2005**, *89*, 5.
(11) Cheng, J. X.; Xie, X. S. *J. Opt. Soc. Am. B* **2002**, *19*, 7.
(12) Woodbury, E. J.; Ng, W. K. *Proc. Inst. Radio Eng. Aust.* **1962**, *50*, 11.
(13) Bloembergen, N. *Am. J. Phys.* **1967**, *35*, 11.
(14) Ploetz, E.; Laimgruber, S.; Berner, S.; Zinth, W.; Gilch, P. *Appl. Phys. B: Lasers Opt.* **2007**, *87*, 3.
(15) Freudiger, C. W.; Min, W.; Saar, B. G.; Lu, S.; Holtom, G. R.; He, C. W.; Tsai, J. C.; Kang, J. X.; Xie, X. S. *Science* **2008**, *322*, 5909.
(16) Ozeki, Y.; Dake, F.; Kajiyama, S.; Fukui, K.; Itoh, K. *Opt. Express* **2009**, *17*, 5.
(17) Nandakumar, P.; Kovalev, A.; Volkmer, A. *New J. Phys.* **2009**, *11*, 033026.
(18) Saar, B. G.; Freudiger, C. W.; Reichman, J.; Stanley, C. M.; Holtom, G. R.; Xie, X. S. *Science* **2010**, *330*, 1368.
(19) Freudiger, C. W.; Min, W.; Holtom, G. R.; Xu, B.; Dantus, M.; Xie, X. S. *Nat. Photonics* **2011**, *5*, 103−109.
(20) Cheng, J. X.; Book, L. D.; Xie, X. S. *Opt. Lett.* **2001**, *26*, 17.
(21) Lu, F.; Zheng, W.; Huang, Z. W. *Appl. Phys. Lett.* **2008**, *92*, 12.
(22) Belanger, E.; Begin, S.; Laffray, S.; De Koninck, Y.; Vallee, R.; Cote, D. *Opt. Express* **2009**, *17*, 21.
(23) Zimmerley, M.; Younger, R.; Valenton, T.; Oertel, D. C.; Ward, J. L.; Potma, E. O. *J. Phys. Chem. B* **2010**, *114*, 10200−10208.
(24) Evans, C. L.; Potma, E. O.; Xie, X. S. N. *Opt. Lett.* **2004**, *29*, 24.
(25) Marks, D. L.; Boppart, S. A. *Phys. Rev. Lett.* **2004**, *92*, 12.
(26) Potma, E. O.; Evans, C. L.; Xie, X. S. *Opt. Lett.* **2006**, *31*, 2.
(27) Jurna, M.; Korterik, J. P.; Otto, C.; Herek, J. L.; Offerhaus, H. L. *Opt. Express* **2008**, *16*, 20.
(28) Fischer, M. C.; Liu, H. C.; Piletic, I. R.; Escobedo-Lozoya, Y.; Yasuda, R.; Warren, W. S. *Opt. Lett.* **2008**, *33*, 3.
(29) Heiman, D.; Hellwarth, R. W.; Levenson, M. D.; Martin, G. *Phys. Rev. Lett.* **1976**, *36*, 4.
(30) Mcmorrow, D.; Lotshaw, W. T.; Kenneywallace, G. A. *IEEE J. Quantum Electron.* **1988**, *24*, 2.
(31) Cho, M. H.; Du, M.; Scherer, N. F.; Fleming, G. R.; Mukamel, S. *J. Chem. Phys.* **1993**, *99*, 4.

(32) Cong, P.; Deuel, H. P.; Simon, J. D. *Chem. Phys. Lett.* **1995**, *240*, 1–3.
(33) Potma, E. O.; de Boeij, W. P.; Wiersma, D. A. *Biophys. J.* **2001**, *80*, 3019.
(34) Guo, L. N.; Tang, Z. L.; Xing, D. *Sci. China, Ser. G: Phys., Mech. Astron.* **2008**, *51*, 788.
(35) Boyd, R. W. *Nonlinear Optics*; Academic Press: Burlington, MA, 2008.
(36) Cheng, J. X.; Xie, X. S. *J. Phys. Chem. B* **2004**, *108*, 3.
(37) Mukamel, S. *Principles of nonlinear optical spectroscopy*; Oxford University Press: New York, 1995.
(38) Ekvall, K.; van der Meulen, P.; Dhollande, C.; Berg, L. E.; Pommeret, S.; Naskrecki, R.; Mialocq, J. C. *J. Appl. Phys.* **2000**, *87*, 5.